Iranian Journal of Catalysis 10(2), 2020, 135-148

IRANIAN JOURNAL OF CATALYSIS

Synthesis of ternary $Ce_2O_3/La_2O_3/Fe_3O_4$ oxides as a potential catalyst for SO_2 reduction by CH_4 to sulfur

Abdol Hossein Khangah[a], Mohammad Javad Sarraf[b], Habib Ale Ebrahim[c], Masoumeh Tabatabaee[d,*]

[a]*Department of Chemical Engineering, Yazd Branch, Islamic Azad University, Yazd, Iran.*
[b]*Department of Chemical and Polymer Engineering, Faculty of Engineering, Yazd University, Yazd, Iran.*
[c]*Department of Chemical Engineering, Amirkabir University of Technology, Tehran, Iran.*
[d]*Departments of Chemistry, Yazd Branch, Islamic Azad University, Yazd, Iran.*

Received 10 October 2019; received in revised form 18 February 2020; accepted 25 February 2020

ABSTRACT

In this study, ternary mixed metal oxide ($Ce_2O_3/La_2O_3/Fe_3O_4$) catalysts were synthesized for reduction of SO_2 to sulfur by CH_4. The response surface method (RSM) was used to optimize the synthesis conditions. The XRD, FESEM, BET, BJH, EDX and NH_3-TPD analyses were performed to characterize the synthesized catalysts. The optimum conditions were obtained for an activated catalyst with 8 wt% La, 16 wt% Fe, and calcination temperature of 650°C. The highest surface area was found to be 71.7 $m^2.g^{-1}$. The validation tests proved that the predicted model was well fitted with the experimental data. Furthermore, the SO_2 conversions were compared at various temperatures (550-800 °C) and it was found that the highest reactivity was found for optimum $Ce_2O_3/La_2O_3/Fe_3O_4$ catalyst. The highest SO_2 conversion was found to be 93% at 800 °C. The catalytic results showed that optimum ternary $Ce_2O_3/La_2O_3/Fe_3O_4$ catalyst had a better performance compared to pure cerium oxide.

***Keywords**: Ternary Cerium/Lanthanum/Iron oxides; Response surface method; Catalyst surface area; Catalytic activity; SO_2 reduction.*

1. Introduction

It is essential to develop effective methods for the removal of sulfur dioxide from environment which is discharged by various industries. Because acid rains are generated from sulfur dioxide gas, they have serious effects on human and animal health, reduce agricultural productivity, cause mortality of fish by reducing the pH of rivers, and lead to many other hazardous effects. Simultaneous removal of SO_2 and NO has been investigated for flue gases containing both gases [1]. Also, in catalytic reduction of NO, the influence of presence of SO_2 was investigated [2-4]. One of the new methods for the removal of sulfur dioxide is catalytic reduction of sulfur dioxide to sulfur. The catalytic and photocatalytic reactions are effective methods for degradation of many pollutants [5-13]. The catalytic reduction is an effective way to remove the sulfur dioxide without the formation of any inappropriate by-products and with the high sulfur selectivity.

*Corresponding author.
E-mail address: tabatabaee@iauyazd.ac.ir (M. Tabatabaee)

Several reducing agents have been investigated for SO_2 reduction, including CO [14], H_2 [15], CH_4 and synthesis gas ($CO+H_2$) [16]. The reduction reactions of sulfur dioxide with these reactants are as follows:

$$2\ CO + SO_2 \longrightarrow 2\ CO_2 + 0.5\ S_2 \quad (1)$$

$$2\ H_2 + SO_2 \longrightarrow 0.5\ S_2 + 2\ H_2O \quad (2)$$

$$CH_4 + 2\ SO_2 \longrightarrow S_2 + CO_2 + 2\ H_2O \quad (3)$$

Among these reactants, CH_4 is more effective than CO and H_2 due to its easy accessibility and low costs for implementation of industrial processes. CH_4 also was studied as reductant agent for production of sulfur from H_2S in catalytic reaction [17]. In literatures, bauxite [18], alumina [19-21], metal oxides and sulfides supported on alumina and activated carbon [22-28], ferromanganese nodules [29], transition metal sulfide [30], cobalt oxide on different supports [31], and ceria based catalysts [32-34] have been investigated as catalysts for SO_2 reduction with CH_4.

Ceria-based metal oxide catalysts are widely used in various industrial processes. However, it is essential to

distinguish safety rules for the use of ceria, therefore, the hazardous effects and cautions should be mentioned. It may damage eyes, skin (itching and skin lesions), digestive system and inhalation system. Also, cerium salts can increase the rate of the blood coagulation. Therefore, precautionary statements are presented as follows. It is forbidden to eat, drink or smoke when this product is using. It is necessary to wear proper respiratory equipment such as air filter and provide ventilation. The modification of cerium oxide with second and third metals improves some catalytic properties such as increase of specific surface area and selectivity in catalytic reactions. From cerium binary oxide catalytic applications, cerium-copper for oxidation reactions [35], cerium-cobalt for ethyl acetate oxidation [36], cerium-yttrium for photocatalytic degradation [37], and cerium-tin for selective catalytic reduction of NO_x by NH_3 [38] have been reported. The addition of third metal on cerium binary oxide can modify the composite properties such as catalytic activity. Various ternary combinations of cerium oxide such as Ce-Ti-Zr, Ce-Cu-Zr, Ce-Mn-Al, Ce-Zr-Nd, Ce-Cu-V mixed oxides have been used for different catalytic applications in literatures [39-44]. However, little attention has been paid to the reduction of SO_2 to sulfur over ternary metal oxides based on cerium oxide. For example, Ce-La-Cu mixed oxide has been used for the reduction of SO_2 to sulfur by methane [32, 45].

It should be mentioned that the optimum conditions for catalyst synthesis were obtained by experimental design. In general, the goal of optimization is to find the conditions that provide the best output [46-48]. Many researchers have investigated the effect of one factor at a time (OFAT) on an experimental response by varying only one factor at a time and fixing other factors. However, OFAT experiments have some disadvantages; and a designed experiment is preferred because of less resources such as time, material, experiments and costs; higher accuracy for estimation of each factor effects and significant interactions between factors [49, 50]. The response surface methodology (RSM) is a powerful statistical-based technique which is applied to interpret the interactions between factors and understand the complex system performance [51-56]. In RSM class, central composite design (CCD) has been applied to fit a quadratic surface which is an appropriate for the optimization of process [52-54]. Thus, in the present work, RSM was selected according to CCD for experimental design.

As mentioned above, little research literature is available from SO_2 reduction over ceria-based metal oxide catalysts. The catalytic performance of ternary $Ce_2O_3/La_2O_3/Fe_3O_4$ oxides has so far not been studied.

In this study, RSM was applied to optimize the surface area of ternary $Ce_2O_3/La_2O_3/Fe_3O_4$ oxides which were synthesized by co-precipitation method for SO_2 reduction to sulfur depending on three parameters containing calcination temperature, La content and Fe content. The synthesized catalysts were characterized by XRD, FESEM, BET, BJH, EDX and NH_3-TPD analyses. Furthermore, other goals of this research were to study the catalytic activity and selectivity for SO_2 reduction to sulfur in the presence of CH_4; and also determine the activation energy.

2. Experimental

2.1. Materials

All chemicals were obtained from Merck. Iron nitrate nonahydrate ($Fe(NO_3)_3.9\ H_2O$), lanthanum nitrate hexahydrate ($La(NO_3)_3.6H_2O$), cerium nitrate hexahydrate ($Ce(NO_3)_3.6H_2O$) and sodium hydroxide (NaOH) were used as initial materials for the synthesis of various catalysts.

2.2. Catalyst preparation

The co-precipitation method was used for catalyst preparation [32, 45]. It should be mentioned that the calculation was based on 10.0 g of metal. For example, a ternary catalyst with 76 wt% Ce, 8 wt% La and 16 wt% Fe was synthesized with 7.6 g of Ce, 0.8 g of La and 1.6 g of Fe which were different from their metal oxides. This catalyst was designated as Ce_2O_3/La_2O_3(8 wt% La)/Fe_3O_4(16 wt% Fe). Other catalysts with different metal contents were marked as mentioned above. To synthesize ternary catalysts, the specific amounts of aqueous cerium nitrate, lanthanum nitrate and iron nitrate were combined under stirring. Then, the precipitated nanoparticles were obtained by addition of NaOH solution as precipitation agent. For example, ternary $Ce_2O_3/La_2O_3/Fe_3O_4$ catalyst with 76 wt% Ce, 8 wt% La and 16 wt% Fe was synthesized as follows. Firstly, 23.6 g of $Ce(NO_3)_3.6H_2O$, 2.5 g of $La(NO_3)_3.6H_2O$ and 11.6 g of $Fe(NO_3)_3.9\ H_2O$ were dissolved in 355 mL deionized water and then stirred for 10 min to obtain a homogeneous solution (solution A). To prepare the solution of precipitation agent, 10.6 g of NaOH was dissolved in 532 mL deionized water (solution B). In this step, the solution of precipitation agent (solution B) was slowly added to the solution A to complete precipitation reaction. Finally, the precipitated nanoparticles were dried overnight at 120 °C in an oven and calcined at 650-780 °C for 3 h in a furnace which can be used as catalyst.

2.3. Catalyst characterization

X-ray diffraction (XRD) patterns of prepared nano-catalysts were recorded on Equinox 3000 instrument from Inel, with an acceleration voltage of 40 kV, and scanning range of 10-118° with a resolution of 0.1°. The average crystal size of catalysts was approximated using both Scherer and Williamson-Hall equations as follows [8, 57-59]:

$$d = \frac{0.9\lambda}{\beta \cos\theta} \quad (4)$$

$$\beta \cos\theta = \frac{0.9\lambda}{d} + 2A\varepsilon \sin\theta \quad (5)$$

where d (nm) represents the crystal size of catalysts; λ is the wavelength (0.15406 nm); β is the peak width at the half maximum and θ denotes the diffraction angle. In Williamson-Hall equation, A and ε are constants which usually are equal to 1.0. It should be mentioned that crystal size in Equation (5) is estimated from the intercept of linear plot of β cos(θ) versus 2sin(θ). To characterize the catalyst particles shape, a field-emission scanning electron microscopy (FESEM) (Hitachi S-4160 scanning microscope) was applied. The specific surface area and N_2 adsorption isotherms of synthesized nano-catalysts were evaluated using BET method at 77 ˚K, by Autosorb-1MP apparatus from Quantachrome. BJH pore size distributions were also obtained from the N_2 adsorption isotherms. Furthermore, the presence of elements in the structure of synthesized catalysts was evaluated by energy dispersive X-ray fluorescence (EDX) analysis using a Tescan Vega/II/XMU instrument. To distinguish total, weak, medium, and strong acidic sites, NH_3-TPD analysis was used with a Nanosord NS91 apparatus.

2.4. Optimization of surface area of catalysts with RSM experimental design

RSM is an applicable method to find the optimal response within the defined ranges of the effective factors [60]. The quadratic regression models can be used to evaluate the system performance [61]. In this study, to obtain the maximum surface area of synthesized ternary catalysts, RSM was applied according to central composite design (CCD). Three factors including calcination temperature (X_1) in the range of 650-750°C, weight percentage of La (X_2), and weight percentage of Fe (X_3) in the range of 8-16 wt% were intended to achieve the best synthesis conditions of ternary catalysts. The factors and levels used for the variables in RSM are given in Table 1. An optimal number of experiments (N) in CCD method can be determined as follows [62, 63]:

$$N = 2^k + 2k + c_p \quad (6)$$

where k is the number of independent variables; 2^k is the factorial points; 2k denotes the axial points and c_p denotes the number of center points applied to evaluate the standard deviation. CCD with 3 specified factors contained 6 axial points, 6 replicates at the center points and 2^3 (8) full factorial tests was used. To fit the experimental data, the quadratic (second order) polynomial model was employed. It is as follows [64-66]:

$$Y = \beta_0 + \sum_{i=1}^{z} \beta_i X_i + \sum_{i=1}^{z-1} \sum_{j=1}^{z} \beta_{ij} X_i X_j + \sum_{i=1}^{z} \beta_{ii} {X_i}^2 \quad (7)$$

where Y is the predicted response; z denotes the number of factors; X_i denotes the input variables; X_iX_j shows the interactions between parameters; X_i^2 denotes the square effect; β_0 is the intercept parameter; β_i denotes the linear term β_{ii} is the second-order term and β_{ij} represent the interaction effects. The adequacy of applied regression models was evaluated by the analysis of variance (ANOVA). The F value and P value at 95% confidence level were used to check the statistical significance of model. The data analysis was performed by using Design-Expert software.

2.5. Catalyst performance tests

The experiments were performed in a fixed-bed stainless steel tubular reactor. For each test, 300 mg of catalyst was put in the catalytic bed. The schematic of the experimental system is shown in Fig. 1. At first, the reactor was purged by an inert gas stream (gas 1). Then, the reactor was heated to reach a desired temperature. The reactant gas (gas 2) is a combination of CH_4, SO_2, and inert (argon) streams with predefined concentrations.

Table 1. The factors and levels used for the variables in RSM.

Factors	Symbol	Levels				
		-α	-1	0	+1	+α
Calcination temperature (°C)	X_1	616	650	700	750	784
Fe content (wt%)	X_2	5.3	8.0	12.0	16.0	18.7
La content (wt%)	X_3	5.3	8.0	12.0	16.0	18.7

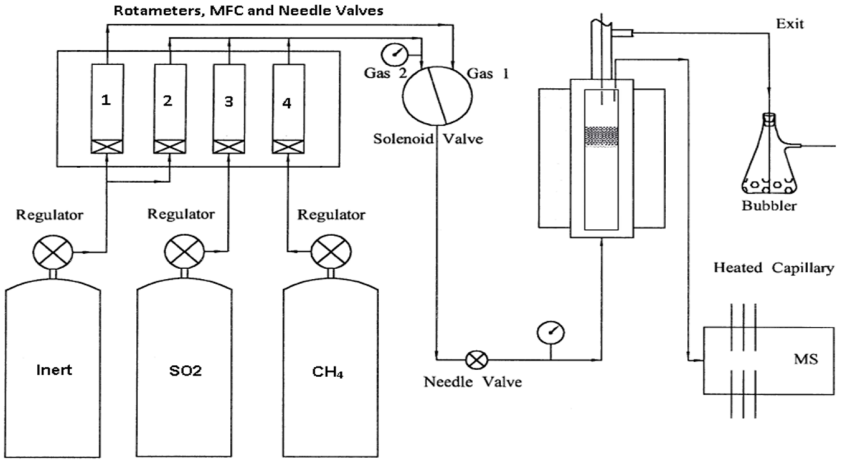

Fig. 1. Flow diagram of the catalytic performance test system.

The inlet concentrations of SO_2, CH_4, and argon gases in the mixture were adjusted by 3 mass flow controllers (MFC). The reaction outlet was analyzed continuously by a mass spectrometer (MS) from Leda Mass. The following expression can be used to calculate the SO_2 conversion:

$$X_{SO2} = \frac{V_{SO2_{in}} - V_{SO2_{out}}}{V_{SO2_{in}}} \times 100 \quad (8)$$

While $V_{SO2_{in}}$ and $V_{SO2_{out}}$ are inlet and outlet SO_2 velocities, respectively.

3. Results and Discussion

3.1. RSM method for BET surface area optimization

Calcination temperature (X_1), La content (wt%) (X_2), and Fe content (wt%) (X_3) were three independent variables which affected the surface area of ternary catalysts. The simultaneous effects of X_1, X_2, and X_3 were investigated by using RSM according to CCD. Table 2 gives the results of predicted and real BET surface areas of synthesized ternary catalysts. The final second order model was obtained from RSM which is shown as follows:

$$Y = 55.57 - 6.748 \times X_1 - 3.033 \times X_2 + 3.715 \times X_3 - 1.650 \times X_1X_2 - 1.183 \times X_1X_3 - 1.840 \times X_2X_3 + 1.058 \times {X_1}^2 - 1.348 \times {X_2}^2 + 1.589 \times {X_3}^2 \quad (9)$$

where Y is the BET surface area of ternary $Ce_2O_3/La_2O_3/Fe_3O_4$ catalysts. The analysis of variance (ANOVA) was used for model validation; and the results are given in Table 3. The calculated and critical F-values were found to be 31.42 and 3.02, respectively ($F_{cal} > F_c$). The greater F_{cal} value confirmed that the applied model was suitable for process modeling [67, 68].

Also, P-value of the second order model was 3.59×10^{-6} (<0.05) approving the good fitting of the model. The F-value of (lack of fit) LOF can be applied to investigate the variation in the experimental data around the model. When this term is insignificant (P-value >0.05 and $F_{cal}<F_c$), the fitted model fits the experimental data well [67-69]. In this study, the P-value, F_{cal}-value and F_c-value of LOF term were 8.34×10^{-2}, 3.83 and 5.05, respectively. The P-value greater than 0.05 ($8.34\times10^{-2}>0.05$) and lower F_c-value of LOF compared to F_{cal}-value ($F_{cal}=3.83<F_c=5.05$) indicated that the fitted model was statistically logic and it was adequate for prediction of BET surface area.

Fig. 2 indicates three diagnostic plots for investigation of the model goodness. Fig. 2 (a) indicates the normal probability plot versus externally studentized residuals. This plot denotes the normal plot of residuals. As observed, the residuals distributed around the normal straight line conforming an appropriate model. The correlation coefficient (R^2) was applied to evaluate the fit of second order model. R^2 value of applied model was found to be 0.97 showing that only 3 % of the total variables were not clarified by the obtained BET surface area. The obtained (S/N) adequate precision was greater than 4 approving remarkably design space [48, 70]. Fig. 2 (b) indicates the predicted versus actual BET surface area of synthesized ternary $Ce_2O_3/La_2O_3/Fe_3O_4$ catalysts. As observed, the most of points were close to the y=x line displaying the correlation of the actual and predicted data. Also, it confirmed that the applied second order model was appropriate for the surface area prediction. The plot of residual versus predicted surface area is illustrated in Fig. 2 (c). As shown, a random scatter was attained in a constant range of ±4.146 that is an allowed range.

Table 2. The actual and predicted BET surface area of ternary $Ce_2O_3/La_2O_3/Fe_3O_4$ catalysts by using RSM according to CCD method.

Runs	Factor X_1	Factor X_2	Factor X_3	Real area (m^2/g)	Predicted area (m^2/g)
1	1	1	-1	47.0	44.8
2	-1	-1	1	71.2	71.7
3	0	0	0	55.5	55.6
4	0	0	0	54.5	55.6
5	0	0	α	65.3	64.0
6	0	0	0	55.0	55.6
7	1	1	1	47.1	46.1
8	0	α	0	45.6	48.6
9	-1	1	-1	58.8	59.2
10	α	0	0	44.1	48.2
11	0	0	0	54.7	55.6
12	-1	1	1	65.8	65.3
13	0	0	0	56.4	55.6
14	0	0	-α	52.3	53.5
15	1	-1	-1	51.7	50.4
16	0	-α	0	55.5	57.2
17	0	0	0	57.8	55.6
18	-1	-1	-1	59.1	58.3
19	-α	0	0	70.5	67.2
20	1	-1	1	61.4	59.2

Table 3. The ANOVA analysis of the fitted second order model for optimization of $Ce_2O_3/La_2O_3/Fe_3O_4$ BET surface area.

Source	Sum of Squares	DF	Mean Square	F-value (F_{cal})	F_c	P-value (Prob> F)	
Model	1081.03	9	120.11	31.42	3.02	3.59×10^{-6}	significant
X_1	621.78	1	621.78	162.68		1.64×10^{-7}	
X_2	125.59	1	125.59	32.86		1.90×10^{-4}	
X_3	188.47	1	188.47	49.31		3.62×10^{-5}	
X_1X_2	21.78	1	21.78	5.69		3.81×10^{-2}	
X_1X_3	11.18	1	11.18	2.92		1.17×10^{-1}	
X_2X_3	27.08	1	27.08	7.08		2.38×10^{-2}	
$(X_1)^2$	16.14	1	16.14	4.22		6.69×10^{-2}	
$(X_2)^2$	26.16	1	26.16	6.84		2.58×10^{-2}	
$(X_3)^2$	36.37	1	36.37	9.51		1.15×10^{-2}	
Residual	38.21	10	3.82				
Lack of Fit	30.30	5	6.06	3.83	5.05	8.34×10^{-2}	not significant
Pure Error	7.91	5	1.58				
Cor Total	1119.24	19					

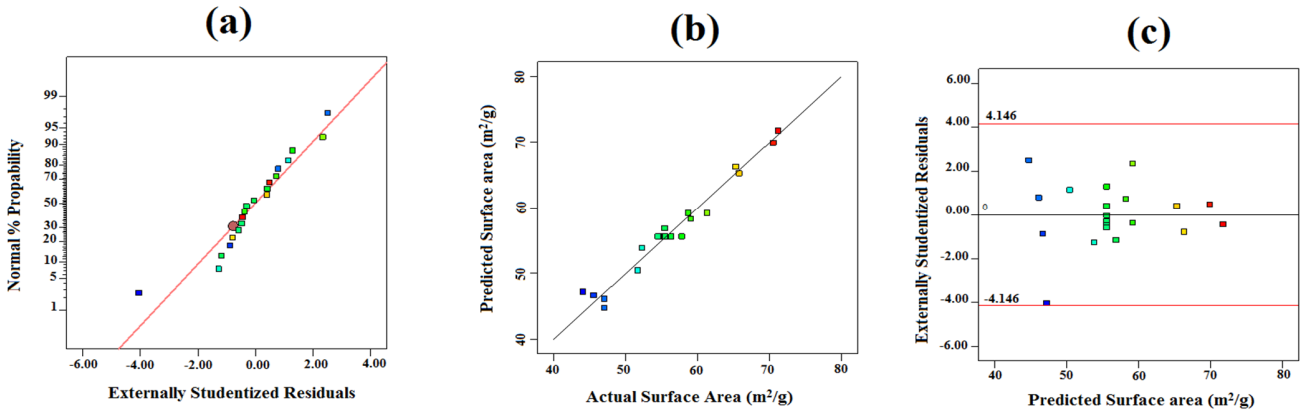

Fig. 2. Three diagnostic plots for the applied quadratic model (a) normal probability plot of residuals; (b) predicted versus actual BET surface area values for ternary $Ce_2O_3/La_2O_3/Fe_3O_4$ catalysts; (c) residuals versus predicted BET surface area values for ternary $Ce_2O_3/La_2O_3/Fe_3O_4$ catalysts.

It should be mentioned that Pareto analysis was applied to investigate the importance of each term (P_i) on the BET surface area as response. It is represented as follows [68, 70]:

$$P_i = \left(\frac{{b_i}^2}{\sum {b_i}^2}\right) \times 100 \ ; (i \neq 0) \qquad \textbf{(10)}$$

The results of Pareto analysis are shown in Fig. 3. As observed, the relative importance of singular factor was in the order of X_1(calcination temperature, 55.9%) > X_3 (Fe weight percentage, 16.9%) > X_2 (La weight percentage, 11.3%). The relative importance of interaction terms was as follows: X_2X_3 (4.2%) > X_1X_2 (3.3%) > X_1X_3 (1.7%); while the following sequence was for relative importance of quadratic terms: X_3^2 (3.1%) > X_2^2 (2.2%) > X_1^2 (1.4%). Thus, the calcination temperature had the most important influence on the BET surface area of ternary $Ce_2O_3/La_2O_3/Fe_3O_4$ catalysts according to Pareto analysis. Also, the sign of calcination temperature coefficient in Equation 8 was negative which stated that the surface area decreased with the increase of calcination temperature. So, a decrease in calcination temperature had a synergistic effect. This can be due to the sintering of ternary metal oxide nanoparticles, blockage of smaller pores and pore collapse at higher calcination temperatures [32, 71]. The importance of calcination temperature can be explained by F-value and P-value of applied second order model. As shown, the highest F-value with P-value lower than 0.05 was obtained for calcination temperature (X1) confirming that this parameter had the most important influence on the BET surface area (Table 3). Furthermore, P-values predicted for variables including X_1, X_2, X_3, X_1X_2, X_2X_3, X_2^2, and X_3^2 were less than 0.05, showing the importance of these variables in the surface area. On the other hand, the variables containing X_1X_3, and X_1^2 were the insignificant terms in the applied second order model because their p-values were greater than 0.05.

The 3D surface plots for BET surface area of ternary $Ce_2O_3/La_2O_3/Fe_3O_4$ catalysts are indicated in Fig. 4. It is possible to find the optimum levels of two corresponding variables based on 3D surface plots. The interaction between calcination temperature and La content (wt%) are illustrated in Fig. 4 (a). As observed, the predicted surface area decreased with increasing the calcination temperature from 650°C to 750°C. The reason can be explained as follows. Indeed, higher calcination temperature led to the sintering of ternary metal oxide nanoparticles, blockage of smaller pores and pore collapse [32, 71]. Also, BET surface area decreased with increasing the La content.

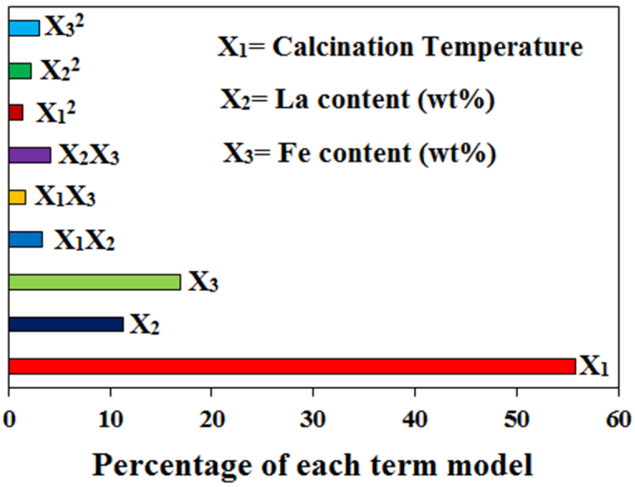

Fig. 3. Pareto analysis to indicate the importance of parameters in the applied quadratic model.

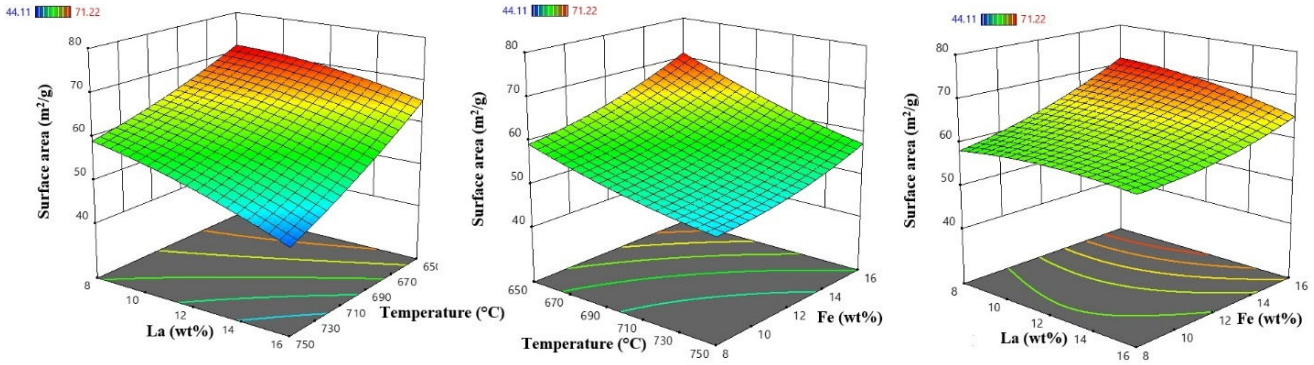

Fig. 4. The 3D surface area plots (a) combined effects of calcination temperature and La content, (b) calcination temperature and Fe content, and (c) La and Fe contents on the prediction of BET surface area for ternary $Ce_2O_3/La_2O_3/Fe_3O_4$ catalysts.

This decrease can be due to the formation of larger crystals for ternary catalysts synthesized with higher La content (> 8wt%) which was confirmed by XRD analysis. Indeed, the nucleation process was slower, and the growth rate was faster at higher La content leading to a decrease in surface area. Furthermore, the agglomeration of nanoparticles may occur during synthesis process higher La content. The highest surface area was achieved at 650˚C and La content of 8.0 wt%. Fig. 4 (b) shows the interaction between calcination temperature and Fe content (wt%) on the BET surface area. As shown, the surface area of ternary catalysts increased with the increase of Fe content (wt%) and decrease of calcination temperature. As mentioned above, the sintering of ternary metal oxide nanoparticles, blockage of smaller pores and pore collapse were stopped at lower calcination temperatures leading to an increase in surface area of catalysts [32, 71]. Really, the crystal growth in ternary catalysts was inhibited in the presence of higher Fe oxides leading to a faster nucleation process. The crystal growth was retarded at higher Fe content because the Fe atomic radius 126 pm is smaller than La (187 pm) and Ce (182 pm) atoms leading to the formation of smaller crystals. The final 3D plot is attributed to the interaction between La and Fe contents on the prediction of BET surface area. As observed, the surface area of ternary catalysts increased with a decrease in La content and an increase in Fe content. The reasons were mentioned above. The optimum BET surface area for ternary catalysts was found to be 71.7 $m^2.g^{-1}$ which achieved at calcination temperature 650°C, La content of 8 wt% and Fe content of 16 wt%. The confirmation experiment was performed under the optimum conditions to validate the applied model. The experimental value of surface area under optimum conditions was found to be 73.5 ($m^2.g^{-1}$) that was in accordance with the predicted value within 2.4% of error. This estimated and acceptable error indicated the validity of the model.

3.2. Characterization of synthesized catalysts

Fig. 5 indicates XRD patterns of Ce_2O_3, Ce_2O_3/La_2O_3(8wt% La)/Fe_3O_4(16wt% Fe) and Ce_2O_3/La_2O_3(12wt% La)/Fe_3O_4(12wt% Fe) catalysts. It should be mentioned that the Miller indexes ((hkl) crystal surfaces) and corresponding peaks were reported according to JCPDS files. As shown, for all samples, the distinct crystal surfaces of cerium oxide phase included (111), (200), (220), (311), (222), (400) and (331) according to JCPDS card no. 65-5923 [72]. A very weak peak at around 2θ=30.7° was attributed to the one of the crystal surfaces of La oxide, namely (101). Also, two other peaks at around 2θ =28.5° and 57.0° related to the (002) and (201) crystal surfaces of La oxide, respectively which were overlapped with the cerium oxide peaks. These crystal surfaces of La oxide were detected according to JCPDS card no. 05-0602 [73]. The crystal surfaces of (311) and (400) were attributed to the weak peaks at around 2θ =35.0 and 43.0, respectively confirming Fe oxide phase according to JCPDS card no. 19-0629 [74]. The XRD results represented that the main structure of ternary catalysts included Ce oxide phase and also confirmed the presence of La and Fe phases as mentioned above. Therefore, XRD results showed that ternary catalysts were successfully synthesized. The average crystal size of ternary Ce_2O_3/La_2O_3(8wt% La)/Fe_3O_4(16wt% Fe) catalyst obtained from Scherer equation (Equation 4) and Williamson-Hall equation (Equation 5) was found to be 8.4 and 10.2 nm, respectively.

Fig. 6 shows the nitrogen adsorption isotherms of pure Ce_2O_3 and ternary catalysts. As shown, ternary Ce_2O_3/La_2O_3(8wt% La)/Fe_3O_4(16wt% Fe) catalyst had the highest nitrogen adsorption. The total pore volume (V_t) of Ce_2O_3, Ce_2O_3/La_2O_3(8wt% La)/Fe_3O_4(16wt% Fe) and Ce_2O_3/La_2O_3(12wt% La)/Fe_3O_4(12wt% Fe) were found to be 0.125, 0.176 and 0.041 cm^3/g, respectively.

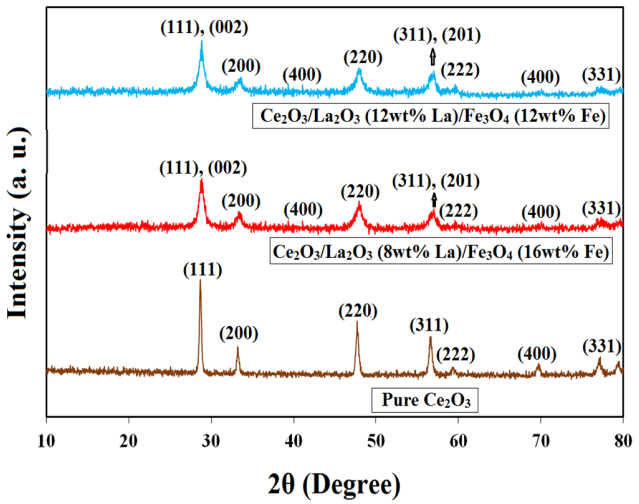

Fig. 5. XRD patterns of Ce_2O_3, Ce_2O_3/La_2O_3(8wt% La)/Fe_3O_4(16wt% Fe), and Ce_2O_3/La_2O_3(2wt% La)/Fe_3O_4(12wt% Fe) catalysts.

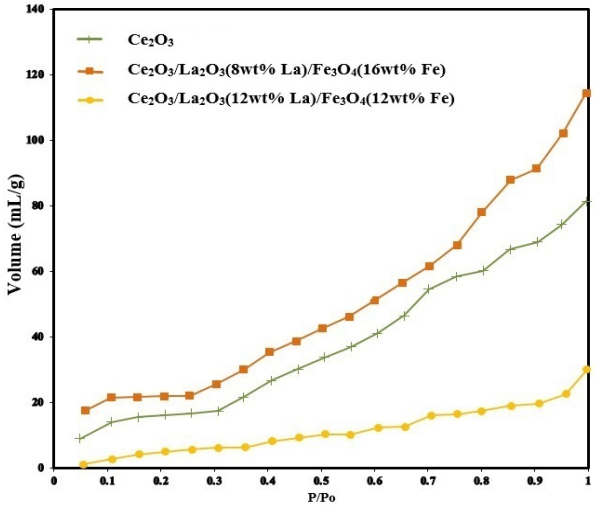

Fig. 6. N_2 adsorption isotherms of Ce_2O_3 and ternary Ce_2O_3/La_2O_3(8wt% La)/Fe_3O_4(16wt% Fe), and Ce_2O_3/La_2O_3(2wt% La)/Fe_3O_4(12wt% Fe) catalysts.

Furthermore, BJH pore size distributions of prepared catalysts are depicted in Fig. 7. It is observed that the greatest amount of mesopores was obtained for Ce_2O_3/La_2O_3(8wt% La)/Fe_3O_4(16wt% Fe). The N_2 adsorption at higher relative pressure (p/p_0) displays the mesoporous adsorption according to IUPAC classification [75, 76]. Therefore, N_2 adsorption of Ce_2O_3/La_2O_3(8wt% La)/Fe_3O_4(16wt% Fe) catalyst at higher p/p_0 was greater than that of Ce_2O_3 and Ce_2O_3/La_2O_3(12wt% La)/Fe_3O_4(12wt% Fe) catalysts confirming the higher mesopores of optimum catalyst. The morphology of pure Ce_2O_3 and optimum Ce_2O_3/La_2O_3(8wt% La)/Fe_3O_4(16wt% Fe) catalyst was investigated by FESEM analysis (Fig. 8).

As shown, the particle size of ternary Ce_2O_3/La_2O_3(8 wt% La)/Fe_3O_4(16 wt% Fe) catalyst was lower than that of pure Ce_2O_3 catalyst due to the difference in crystallization step.

Fig. 9 shows the EDX analysis of pure Ce_2O_3 and ternary Ce_2O_3/La_2O_3(8 wt% La)/Fe_3O_4(16 wt% Fe) catalysts. The presence of Ce, La, O and Fe elements in the ternary $Ce_2O_3/La_2O_3/Fe_3O_4$ catalysts was confirmed by EDX analysis. As observed in Fig. 9 (a), distinct Ce and O peaks existed in EDX analysis of Ce_2O_3. Furthermore, La and Fe peaks appeared in EDX analysis of Ce_2O_3/La_2O_3(8 wt% La)/Fe_3O_4(16 wt% Fe) catalyst. The presence of these peaks confirmed that ternary catalyst was successfully provided.

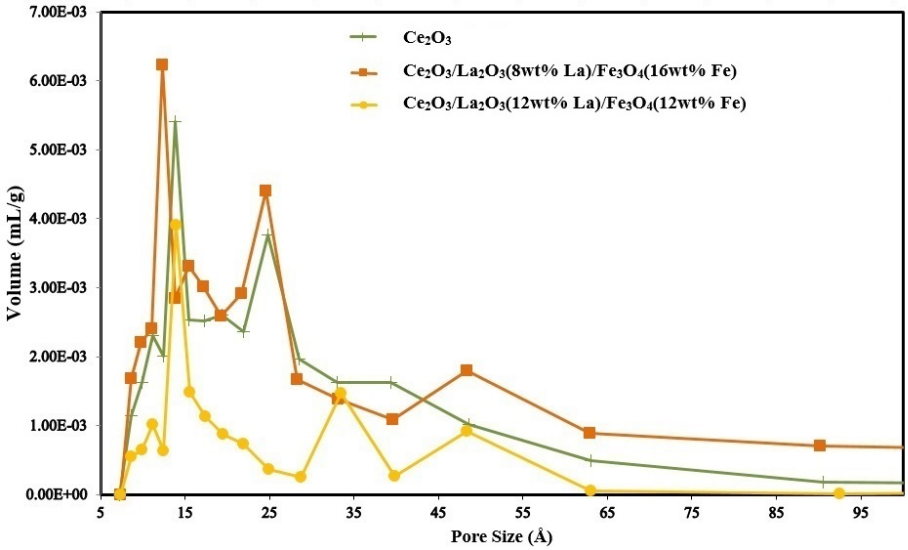

Fig. 7. BJH pore size distribution of Ce_2O_3 and ternary Ce_2O_3/La_2O_3(8wt% La)/Fe_3O_4(16wt% Fe), and Ce_2O_3/La_2O_3(2wt% La)/Fe_3O_4(12wt% Fe) catalysts.

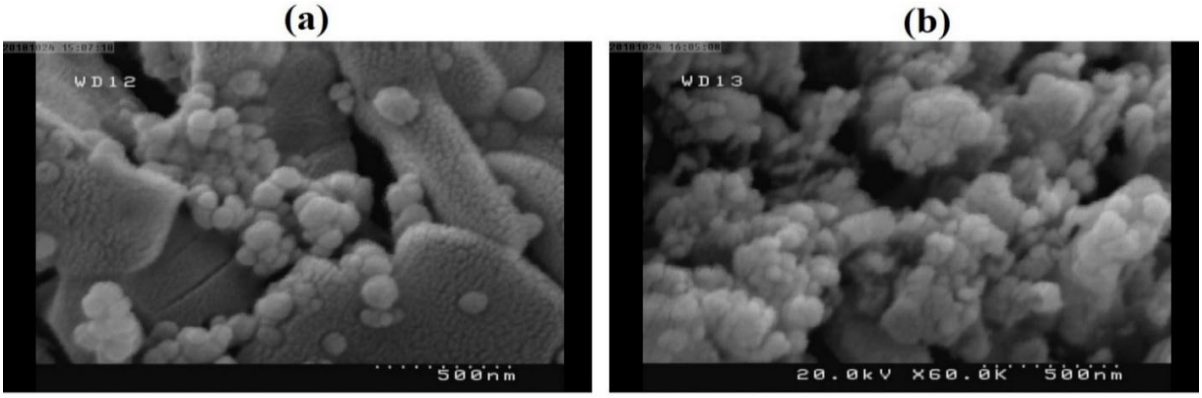

Fig. 8. FESEM images (a) Ce_2O_3 and (b) ternary Ce_2O_3/La_2O_3(8wt% La)/Fe_3O_4(16wt% Fe) catalysts.

However, based on quantitative analysis, Ce, La and Fe weight percentage was found to be 61.02, 6.13 and 12.29 wt% for ternary Ce_2O_3/La_2O_3(8 wt% La)/Fe_3O_4(16 wt% Fe); and Ce percentage was found to be 82.6 wt% for pure Ce_2O_3 catalyst. It is necessary to mentioned that the values obtained from EDX analysis were lower than respected values. This can be due to the presence of excess sodium during co-precipitation method and the presence of impurity peaks. Furthermore, gold coating of sample surfaces led to the existence of Au peak in EDX analysis.

NH_3-TPD analysis was applied to determine the weak, moderate, and strong acidic sites of synthesized Ce_2O_3 and ternary Ce_2O_3/La_2O_3(8wt% La)/Fe_3O_4(16wt% Fe) catalysts (Fig. 10). As observed, three temperature regions were assigned to the weak, moderate, and strong acidic sites. The first temperature region at lower temperature corresponded to the weakly bonded NH_3, the second temperature region was attributed to the moderate acid sites, and the third higher temperature region was assigned to the strongly bonded NH_3. The details of temperature regions and the amount of acidic sites are shown in Table 4. As can be seen, weak, moderate and total acid sites of ternary Ce_2O_3/La_2O_3(8wt% La)/Fe_3O_4(16wt% Fe) catalyst was greater than that of pure cerium oxide. This can be due to the electron structure of cationic sites (Ce, La and Fe) exposed on the catalyst surface. The highest change in acidic sites was assigned to the moderate acid sites. The moderate acid sites were found to be 0.283 and 0.758 mmol/g for pure Ce_2O_3 catalyst and ternary catalysts, respectively. Furthermore, the total acid sites of Ce_2O_3 and Ce_2O_3/La_2O_3(8wt% La)/Fe_3O_4(16wt% Fe) catalysts were 0.683 and 0.988 mmol/g, respectively.

3.3. Catalysts activity comparison tests

Methane is a suitable reactant for sulfur dioxide reduction to sulfur. The main reaction between methane and sulfur dioxide is given as follows:

$$CH_4 + 2\ SO_2 \longrightarrow S_2 + CO_2 + 2\ H_2O \qquad (11)$$

The main side reaction for this process is given by the following reaction:

$$SO_2 + 2\ CH_4 \longrightarrow H_2S + 2\ CO + 3\ H_2 \qquad (12)$$

This side reaction can produce H_2S, which is a very dangerous by-product.

Fig. 11 shows the effect of reactor temperature on SO_2 conversion for cerium oxide, optimum, and minimum mixed oxide catalysts. As observed, for all catalysts, SO_2 conversions increased sharply with the increase of temperature. The performance of cerium oxide did not differ significantly from ternary Ce_2O_3/La_2O_3(12wt% La)/Fe_3O_4(12wt% Fe) catalyst.

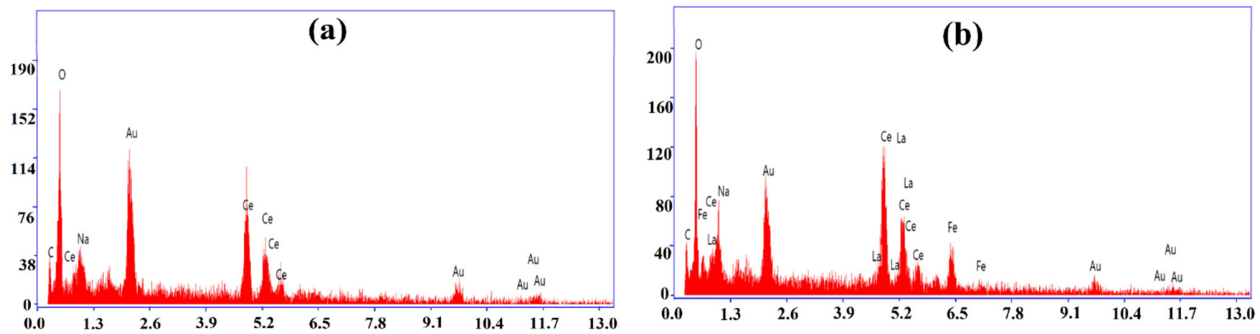

Fig. 9. EDX of (a) Ce_2O_3 and (b) ternary Ce_2O_3/La_2O_3(8wt% La)/Fe_3O_4(16wt% Fe) catalysts.

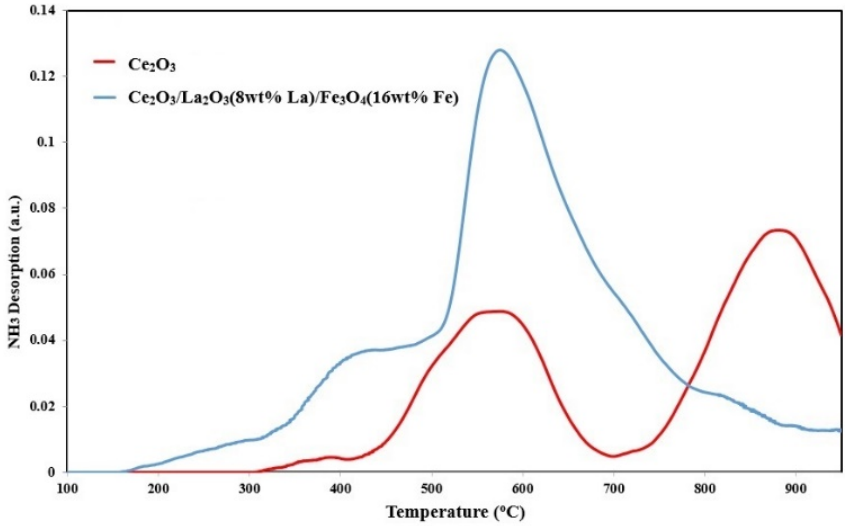

Fig. 10. NH_3-TPD profiles of Ce_2O_3 and Ce_2O_3/La_2O_3(8wt% La)/Fe_3O_4(16wt% Fe) catalysts.

Table 4. The amount of total, weak, moderate, and strong acid sites of catalysts

Sample	Weak acid sites (mmol/g)	moderate acid sites (mmol/g)	Strong acid sites (mmol/g)	Total acid sites (mmol/g)
Ce_2O_3	25-410 °C 0.0108	410-700 °C 0.2829	700-950 °C 0.3896	0.6834
Ce-La-Fe Oxide	25-451 °C 0.1462	451-800 °C 0.7583	800-950 °C 0.0830	0.9875

While the best catalytic performance was obtained for optimum Ce_2O_3/La_2O_3(8wt% La)/Fe_3O_4(16wt% Fe) catalyst. The higher specific surface area and so, higher active sites of optimum catalyst were available for the reaction. These active sites led to a sharp increase in conversion rates.

The partial pressure curves for H_2S and COS undesirable by-products at different temperatures were compared for all catalysts in Fig. 12 (a) and Fig. 12 (b).

As shown in Fig. 12, the amount of H_2S and COS for all catalysts increased with the increase of temperature. It should be mentioned that H_2S production was much higher than COS production. But the increase rate of COS with temperature was higher.

This increase may be due to CS_2 production as follows [27, 32]:

$$CH_4 + S_2 \longrightarrow CS_2 + 2H_2 \quad (\mathbf{13})$$

This produced CS_2 can react with the water produced from reaction (11) and produces H_2S and COS as shown in reaction (14).

$$CS_2 + H_2O \longrightarrow COS + H_2S \quad (\mathbf{14})$$

Moreover, H_2S can be produced by other side reactions:

$$3H_2 + SO_2 \longrightarrow H_2S + 2H_2O \quad (\mathbf{15})$$

$$2H_2 + S_2 \longrightarrow 2H_2S \quad (\mathbf{16})$$

For COS, the other side reaction can also produce COS as follows:

$$CS_2 + CO_2 \longrightarrow 2COS \quad (\mathbf{17})$$

It should be noticed that reaction (16) can be accelerated around temperature of 650 °C. The required hydrogen for reaction (15) and (16) can be supplied by reaction (13) and methane decomposition reaction:

$$CH_4 \longrightarrow C + 2H_2 \quad (\mathbf{18})$$

The required CO_2 for the reaction (17) can be supplied by the reaction (3).

In all temperatures, the amount of H_2S was higher than COS amount, and H_2S was the main side product, because carbonyl sulfide is converted to hydrogen sulfide by the following reaction:

$$COS + H_2O \longrightarrow CO_2 + H_2S \quad (\mathbf{19})$$

It is given that water is readily available due to reaction 1, the occurrence probability of this side reaction is high.

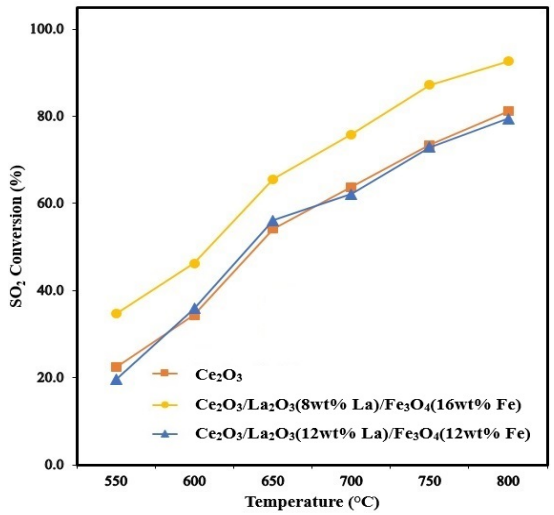

Fig. 11. SO_2 conversion as a function of temperature for different catalysts (feed compositions = 2% SO_2, 1% CH_4, 97% Ar; space velocity = 3000 mL/h^{-1}).

In terms of the production of side products, selectivity and conversion, the optimum catalyst of $Ce_2O_3/La_2O_3/Fe_3O_4$ showed the best performance. This can be due to the higher active area of optimum catalyst. So, the reaction of sulfur dioxide with methane (reaction 1) is preferred (Fig. 11). This leads to a lower availability of methane and sulfur dioxide and thus, side reactions such as reaction (12) are less likely to occur. As a result, inappropriate side products were less produced for optimum catalyst.

The following mechanism was suggested for SO_2 reduction over ternary $Ce_2O_3/La_2O_3/Fe_3O_4$ catalyst. A methane molecule adsorbs on the catalyst surface in the operating temperatures and then reacts with lattice oxygen atom which is neighbor of La or Fe atoms to form an activated methyl radical. The mentioned La and Fe atoms act as Lewis acid sites. The produced methyl radical (CH_3^*) has free electron which occupy these Lewis acid sites. Indeed, after CH_4 adsorption, a dissociation of C−H bond occurs leading to the formation of Fe−CH3 (CH_3^*) or La−CH_3 (CH_3*) and O−H (H^*) species. La−CH_3 (CH_3^*) and Fe−CH_3 (CH_3^*) react with SO_3^{2-} ions that are produced from SO_2 adsorption on ceria [77].

3.4. Determination of activation energy

Activation energies can be determined by Arrhenius equation [78]:

$$\log(k_i) = \log(A_i) - \frac{E_i}{RT} \qquad (20)$$

where R = 8.314 J/mol.K is the gas constant, T (K) and A_i are absolute temperature and pre-exponential constant, respectively.

Arrhenius plot obtained from SO_2 conversion for Ce_2O_3/La_2O_3(8wt% La)/Fe_3O_4(16wt% Fe) catalyst is presented in Fig. 13. The activation energy obtained from Fig. 13 in temperature range of 550-800°C was estimated to be 29718 $kJmol^{-1}$.

3.5. Characterization of catalysts after catalytic tests

The XRD patterns of all catalysts after catalytic tests are indicated in Fig. 14. The results showed that the main peaks and structure of pure Ce_2O_3 and Ce_2O_3/La_2O_3(8wt% La)/Fe_3O_4(16wt% Fe) and Ce_2O_3/La_2O_3(12wt% La)/Fe_3O_4(12wt% Fe) catalysts were preserved after catalytic tests. Nevertheless, the peak intensity of all catalysts after reactor tests was slightly lower than that of fresh catalysts. Furthermore, the EDX results of all catalysts after reactor tests are shown in Fig. 15.

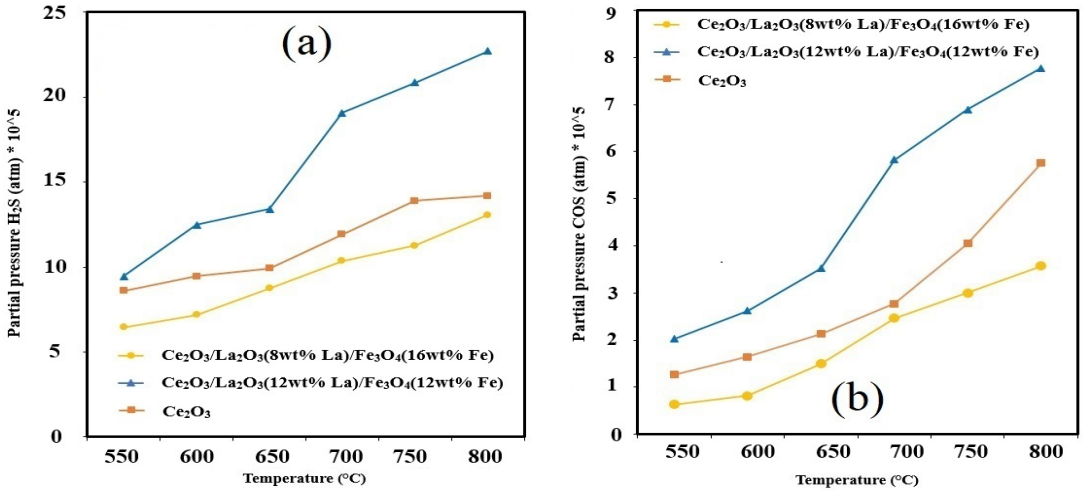

Fig. 12. Partial pressures of H_2S (a) and COS (b) versus temperature for different catalysts (feed compositions = 2% SO_2, 1% CH_4, 97% Ar; space velocity = 3000 mL/h^{-1}).

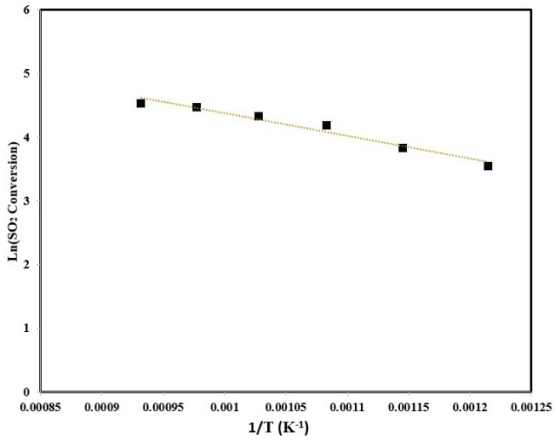

Fig. 13. Arrhenius plots for SO_2 reactions with CH_4 for Ce_2O_3/La_2O_3(8wt% La)/Fe_3O_4(16wt% Fe) catalyst.

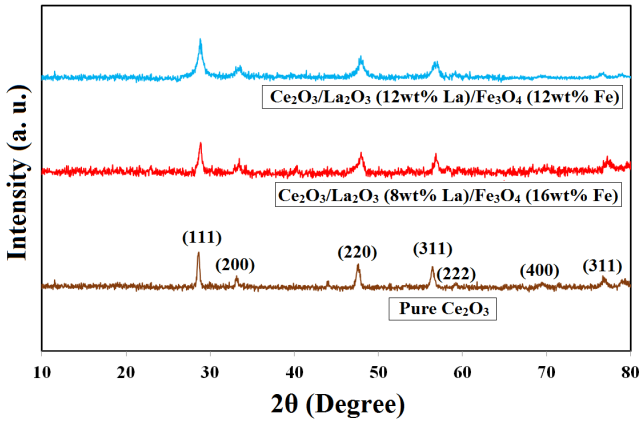

Fig. 14. XRD patterns of spent Ce_2O_3 and ternary $Ce_2O_3/La_2O_3/Fe_3O_4$ catalysts.

The results indicated the presence of the Ce, La, Fe and O in the structure of catalysts. The weight percentage of Ce, La and Fe was 60.12, 5.93 and 12.02 wt% for ternary Ce_2O_3/La_2O_3(8 wt% La)/Fe_3O_4 (16 wt% Fe) which did not change significantly compared to quantitative analysis before reactor tests. This confirmed that the structure of spent catalyst was preserved after tests.

3.6. Comparison of different ternary catalysts

SO_2 conversion and sulfur selectivity for different ternary oxide catalysts have been compared in Table 5. In a study reported by Zhu et al. [33], full SO_2 conversion rate was obtained for Ce/La(4.5)/Cu(5) and Ce/La(4.5)/Ni(5) catalysts at 725 °C. But sulfur selectivity for Ce/La(4.5)/Cu(5) and Ce/La(4.5)/Ni(5) catalysts were found to be 31 and 41%, respectively. In other study conducted by Mousavi et al. [32], SO_2 conversion was found to be 85 and 93% at750 °C for Ce/La(15)/Cu(5) and Ce/La(10)/Ni(5) catalysts, respectively; and the selectivity for these catalysts was low. In our previous study, SO_2 conversion was found to be was 85% for Ce/La(10)/Co(8) catalyst at 750 °C, while the selectivity for the desired product was high (98%). In this study, by replacing iron with cobalt, the selectivity remained at the appropriate level of 98%, while the conversion rate increased to 87%.

4. Conclusions

Ternary $Ce_2O_3/La_2O_3/Fe_3O_4$ catalysts synthesized by co-precipitation method were optimized by using RSM for SO_2 reduction. The optimum surface area was obtained at calcination temperature of 650°C, La content of 8.0 wt% and Fe content of 16.0 wt%. The ANOVA results indicated that the applied quadratic model was adequate for prediction of BET surface area. Among three factors applied in RSM method, the calcination temperature had the most important influence on the BET surface area of ternary catalysts according to Pareto analysis. Also, the surface area of ternary catalysts increased with a decrease in La content and an increase in Fe content. Furthermore, the synthesized pure Ce_2O_3 and ternary catalysts were characterized by BET, BJH, XRD, FESEM, EDX and NH_3-TPD analysis. Therefore, characterization results showed that ternary catalysts were successfully synthesized.

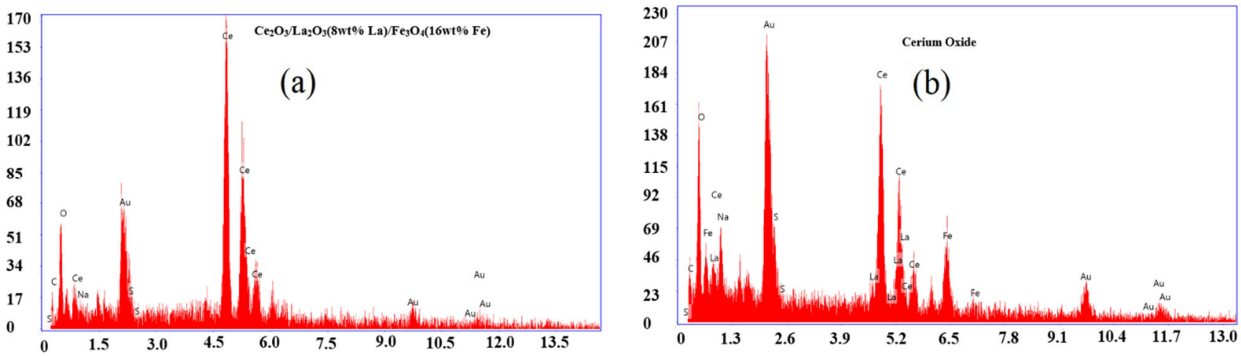

Fig. 15. EDX patterns of spent (a) Ce_2O_3 and (b) ternary Ce_2O_3/La_2O_3(8wt% La)/Fe_3O_4(16wt% Fe) catalysts.

Table 5. SO_2 conversions and sulfur selectivity for different ternary oxide catalysts.

Catalyst	Conversion (%)	Selectivity	Temperature (°C)	Ref.
Ce/La(15)/Cu(5)	85	31	750	[32]
Ce/La(10)/Ni(5)	93	47	750	[32]
Ce/La(4.5)/Cu(5)	100	56	725	[33]
Ce/La(4.5)/Ni(5)	100	34	725	[33]
Ce/La(10)/Co(8)	85	98	750	[78]
Ce/La(8)/Fe(16)	87	98	750	Current study

The results of catalytic tests showed that SO_2 conversion for ternary Ce_2O_3/La_2O_3(8 wt% La)/Fe_3O_4(16 wt% Fe) catalyst was greater than pure cerium oxide. Moreover, the sulfur selectivity for the mentioned optimum catalyst was greater than other catalysts. The lowest undesired by-products such as H_2S and COS were obtained for ternary Ce_2O_3/La_2O_3(8 wt% La)/Fe_3O_4(16 wt% Fe) catalyst. The results confirmed that an increase in specific surface area led to an improvement in catalytic performance for the optimum catalyst.

References

[1] J. Sun, L. Li, G. Zhou, X. Wang, L. Zhang, Y. Liu, J. Yang, X. Lü, F. Jiang, Environ. Sci. Technol. 52 (2018) 4754-4762.

[2] Q. Liang, J. Li, H. He, T. Yue, L. Tong, J. Environ. Sci. 90 (2020) 253-261.

[3] L. Zhao, S. Yang, J. Duan, Q. Liu, Fuel 263 (2020) 116668.

[4] W. Zhang, G. Liu, J. Jiang, Y. Tan, Q. Wang, C. Gong, D. Shen, C. Wu, Chemosphere 243 (2020) 125419.

[5] A. Rostami-Vartooni, A. Moradi-Saadatmand, M. Bagherzadeh, M. Mahdavi, Iran. J. Catal. 9 (2019) 27-35.

[6] B. Divband, A. Jodaei, M. Khatamian, Iran. J. Catal. 9 (2019) 63-70.

[7] T. Feng, P. Zhou, X. Zhao, L. Li, X. Xia, S. Zhang, J. Li, L. Wang, C. Ma, Energy & Fuels 33 (2019) 7491-7499.

[8] S. Dianat, Iran. J. Catal. 8 (2018) 121-132.

[9] L. Shabani, H. Aliyan, Iranian J. Catal. 6 (2016) 221-228.

[10] S. Aghabeygi, R.K. Kojoori, H.V. Azad, Iran. J. Catal. 6 (2016) 275-279.

[11] H. Pouretedal, A. Sohrabi, J. Iran. Chem. Soc. 13 (2016) 73-79.

[12] M. Barjasteh-Moghaddam, A. Habibi-Yangjeh, J. Iran. Chem. Soc. 8 (2011) S169-S175.

[13] N. Assi, P.A. Azar, M.S. Tehrani, S.W. Husain, J. Iran. Chem. Soc. 13 (2016) 1593-1602.

[14] T. Feng, P. Zhou, X. Zhao, L. Li, X. Xia, S. Zhang, J. Li, L. Wang, C. Ma, Energy & Fuels 33 (2019) 7491-7499.

[15] T. Feng, M. Huo, X. Zhao, T. Wang, X. Xi, C. Ma, Chem. Eng. Res. Des. 121 (2017) 191-199.

[16] T. Ge, C. Zuo, J. Zhang, L. Wei, C. Li, Ind. Eng. Chem. Res. 57 (2018) 4170-4179.

[17] T. Kane, J. Guerrero-Caballero, A. Löfberg, Appl. Catal. B Environ. 265 (2020) 118566.

[18] J. J. Helstrom, G.A. Atwood, Ind. Eng. Chem. Proc. Des. Dev. 17 (1978) 114-117.

[19] A. Bobrin, V. Anikeev, A. Yermakova, V. A. Kirillov, React. Kinet. Catal. Lett. 40 (1989) 363-367.

[20] J. Sarlis, D. Berk, Ind. Eng. Chem. Res. 27 (1988) 1951-1954.

[21] A. Bobrin, V. Anikeev, A. Yermakova, V. Zheivot, V.A. Kirillov, React. Kinet. Catal. Lett. 40 (1989) 357-362.

[22] D. J. Mulligan, D. Berk, Ind. Eng. Chem. Res. 31 (1992) 119-125.

[23] D. J. Mulligan, K. Tam, D. Berk, Canadian J. Chem. Eng. 73 (1995) 351-356.

[24] T. S. Wiltowski, K. Sangster, W.S. O'Brien, J. Chem. Technol. Biotechnol. 67 (1996) 204-212.

[25] J. Sarlis, D. Berk, Chem. Eng. Commun. 140 (1995) 73-85.

[26] X. Zhang, D. O. Hayward, C. Lee, D. M. P. Mingos, Appl. Catal. B Environ. 33 (2001) 137-148.

[27] S. E. Mousavi, H. Pahlavanzadeh, M. Khani, H. Ale Ebrahim, A. Mozaffari, React. Kinet. Mech. Catal. 124 (2018) 669-682.

[28] M. Khani, S. E. Mousavi, H. Pahlavanzadeh, H. Ale Ebrahim, A. Mozaffari, Environ. Sci. Pollut. Res. 26 (2019) 9686-9696.

[29] N. Shikina, S. Khairulin, S. Yashnik, T. Teryaeva, Z. R. Ismagilov, Eurasian Chem. Tech. 17 (2015) 129-136.

[30] D. J. Mulligan, D. Berk, Ind. Eng. Chem. Res. 28 (1989) 926-931.

[31] J. J. Yu, Q. Yu, Y. Jin, S. G. Chang, Ind. Eng. Chem. Res. 36 (1997) 2128-2133.

[32] S. E. Mousavi, H. Ale Ebrahim, M. Edrissi, Synt. React. Inorgan. Metal-Organ. Nano-Metal Chem. 44 (2014) 881-890.

[33] T. Zhu, L. Kundakovic, A. Dreher, Catal. Today 50 (1999) 381-397.

[34] M. Flytzani-Stephanopoulos, T. Zhu, Y. Li, Catal. Today 62 (2000) 145-158.

[35] M. Piumetti, S. Bensaid, T. Andana, N. Russo, R. Pirone, D. Fino, Appl. Catal. B Environ. 205 (2017) 455-468.

[36] M. Konsolakis, S. Carabineiro, G. Marnellos, M. Asad, O. Soares, M. Pereira, J. Órfão, J. Colloid Interf. Sci. 496 (2017) 141-149.

[37] C. M. Magdalane, K. Kaviyarasu, J. J. Vijaya, B. Siddhardha, B. Jeyaraj, J. Kennedy, M. Maaza, J. Alloys Compounds 727 (2017) 1324-1337.
[38] Z. Liu, X. Feng, Z. Zhou, Y. Feng, J. Li, Appl. Surf. Sci. 428 (2018) 526-533.
[39] C. Shan, Y. Xu, M. Hua, M. Gu, Z. Yang, P. Wang, Z. Lu, W. Zhang, B. Pan, Chem. Eng. J. 338 (2018) 261-270.
[40] Z. Shi, Q. Tan, D. Wu, Mater. Chem. Phys. 219 (2018) 263-272.
[41] X. F. Dong, H. B. Zou, W. Lin, Int. J. Hydr. Energy 31 (2006) 2337-2344.
[42] X. Wu, S. Liu, D. Weng, F. Lin, R. Ran, J. Hazard. Mater. 187 (2011) 283-290.
[43] Q. Wang, G. Li, B. Zhao, R. Zhou, J. Hazard. Mater. 189 (2011) 150-157.
[44] R. Cousin, S. Capelle, E. Abi-Aad, D. Courcot, A. Aboukaïs, Appl. Catal. B 70 (2007) 247-253.
[45] S.E. Mousavi, H. Pahlavanzadeh, H. Ale Ebrahim, e-J Surf. Sci. Nanotechnol. 15 (2017) 87-92.
[46] P.W. Araujo, R.G. Brereton, TrAC Trends Anal. Chem. 15 (1996) 63–70.
[47] H.R. Pouretedal, M. Fallahgar, F. Sotoudeh Pourhasan, M. Nasiri, Iran. J. Catal. 7 (2017) 317-326.
[48] N.E. Fard, R. Fazaeli, Iran. J. Catal. 8 (2018) 133-141.
[49] V. Czitrom, American Statistician 53 (1999) 126-131.
[50] R. Leardi, Anal. Chim. Acta 652 (2009) 161-172.
[51] A. L. Ahmad, S. C. Low, S.R. A. Shukor, A. Ismail, Sep. Purif. Tech. 66 (2009) 177–186
[52] M. Kasiri, H. Aleboyeh, A. Aleboyeh, Environ. Sci. Technol. 42 (2008) 7970-7975.
[53] A. Asghar, A. Raman, A. Aziz, W.M.A.W. Daud, Sci. World J. Article ID: 869120 (2014) 1-14.
[54] M. Galedari, M.M. Ghazi, S.R. Mirmasoomi, Chem. Eng. Res. Design 145 (2019) 323-333.
[55] M. Joshaghani, D. Yazdani, A.A. Zinatizadeh, J. Iran. Chem. Soc. 14 (2017) 2449-2456.
[56] A.S. Ertürk, J. Iran. Chem. Soc. 15 (2018) 1685-1698.
[57] S. Aghdasi, M. Shokri, Iran. J. Catal. 6 (2016) 481-487.
[58] S.D. Khairnar, M.R. Patil, V.S. Shrivastava, Iran. J. Catal. 8 (2018) 143-150.
[59] T. Tamiji, A. Nezamzadeh-Ejhieh, J. Taiwan Institute Chem. Eng. 104 (2019) 130-138.
[60] F. Geyikçi, E. Kılıç, S. Çoruh, S. Elevli, Chem. Eng. J. 183 (2012) 53-59.
[61] M. Khayet, C. Cojocaru, M. Essalhi, J. Membr. Sci. 368 (2011) 202-214.
[62] A. Özer, G. Gürbüz, A. Çalimli, B.K. Körbahti, J. Hazard. Mater. 152 (2008) 778-788.
[63] M. Talebi, S. Abbasizadeh, A.R. Keshtkar, Process Safety Environ. Protect. 109 (2017) 340-356.
[64] G. H. Mirzabe, A. R. Keshtkar, J. Ind. Eng. Chem. 26 (2015) 277-285.
[65] F. Gönen, Z. Aksu, J. Hazard. Mater. 154 (2008) 731-738.
[66] A. Najafpoor, H. Alidadi, H. Esmaeili, T. Hadilou, M. Dolatabadi, A. Hosseinzadeh, M. Davoudi, Asia-Pacific J. Chem. Eng. 11 (2016) 258-270.
[67] M. Nosuhi, A. Nezamzadeh-Ejhieh, Electrochim. Acta 223 (2017) 47-62.
[68] T. Tamiji, A. Nezamzadeh-Ejhieh, J. Electroanal. Chem. 829 (2018) 95-105.
[69] H. Derikvandi, A. Nezamzadeh-Ejhieh, J. Colloid Interf. Sci. 490 (2017) 652-664.
[70] H. Derikvandi, A. Nezamzadeh-Ejhieh, J. Colloid Interf. Sci. 490 (2017) 628-641.
[71] Y. Ding, C. Zhao, Y. Li, Z. Ma, X. Lv, Quim. Nova 41 (2018) 1156-1161.
[72] B. Choudhury, P. Chetri, A. Choudhury, RSC Adv. 4 (2014) 4663-4671.
[73] R. Shi, F. Wang, Y. Li, X. Huang, W. Shen, Green Chem. 12 (2010) 108-113.
[74] A. Ruíz-Baltazar, R. Esparza, G. Rosas, R. Pérez, J. Nanomater. 16 (2015) 202.
[75] S. Abbasizadeh, R. Karimzadeh, Micro. Meso. Mater. 266 (2018) 132-140.
[76] S. Abbasizadeh, R. Karimzadeh, Res. Chem. Intermed. 45 (2019) 955-972.
[77] A. H. Khangah, M. J. Sarraf, H. Ale Ebrahim, M. Tabatabaeee, e-J Surf. Sci. Nanotechnol. 17 (2019) 16−26.
[78] S. H. Guiance, I. Coria, I. Irurzun, E. Mola, Chem. Phys. Lett. 660 (2016) 123-126.